Article

Intensification of extreme cold events in East Asia in response to global mean sea-level rise

Check for updates

Caoyi Dong [1,2], Zhongshi Zhang [3,4,5] ✉, Noel Keenlyside [6,7], Stefan Pieter Sobolowski [8,9], Odd Helge Otterå [8,9], Antonio Bonaduce [7], Jiping Xie [7], Roshin P. Raj [7], Yong Liu [1,2], Bo Liu [10] & Mingna Wu [1,2]

Today, the global mean sea level (GMSL) stands ~ 20 cm higher than at the beginning of the last century, and the rate of sea-level rise has been accelerating in recent decades. Even a slight, globally uniform sea-level rise can notably impact atmospheric and oceanic circulations at climatic and potentially synoptic scales. However, the extent to which sea-level rise will influence extreme weather remains largely unknown. Here, we focus on East Asia and conduct climate model experiments to investigate the effects of GMSL rise on winter cold extremes. Our experiments demonstrate that GMSL rise promotes stronger and more frequent extreme cold events, and this influence is expected to strengthen significantly in the coming century. This effect is attributed to weakened mid-high latitude westerly winds and increased occurrence of blocking events over Eurasia. Our study presents evidence that GMSL rise can modify synoptic systems and intensify extreme events, suggesting that both coastal and inland countries are exposed to threats arising from GMSL rise.

Global mean sea level (GMSL) rise is a non-negligible factor in present and future climate systems. GMSL has risen by ~0.2 m over the past century and is projected to rise further by 0.38 m (0.77 m) by 2100 under the SSP1–1.9 (Shared Socio-economic Pathways; SSP5–8.5) scenarios[1], reflecting sea-level commitment from past, present and future emissions[2]. Observations reveal that the rise of GMSL over the past century has magnified flooding in coastal regions[3]. Furthermore, recent research indicates that this slight (in tens of centimeters) globally uniform sea-level rise is strong enough to alter large-scale atmospheric and oceanic circulations[4], particularly at mid-high latitudes. As a result, GMSL rise can modulate global climate and potentially impact regional weather systems. However, how sea-level rise influences synoptic systems or extreme weather/climate events is largely unknown.

Here, we use winter extreme cold events in East Asia as an example to address the impact of sea-level rise on synoptic systems. In recent years, East Asia has experienced unprecedented cold winters and increased extreme weather events[5–7]. For example, in 2020/2021, an extreme cold event occurred, resulting in record-breaking low temperatures at over 60 meteorological stations in China and causing local transportation and electric systems to break down[8–11]. In 2022/2023, an extreme cold event killed at least four persons in Japan and the Korean Peninsula[12,13]. Moreover, in December 2023, numerous regions in China witnessed the largest recorded temperature drop. Recent studies suggest that these extreme cold events were linked to large-scale atmospheric circulation anomalies—such as Ural blocking—which are modulated by Arctic Sea ice[14–21] and oceanic variability in the Atlantic and Pacific[22–25].

[1]Department of Atmospheric Science, School of Environmental Studies, China University of Geoscience, Wuhan, China. [2]Centre for Severe Weather and Climate and Hydro-geological Hazards, Wuhan, China. [3]Department of Atmospheric and Oceanic Sciences, School of Physics, Peking University, Beijing, China. [4]School of Geographic Science, Nantong University, Nantong, China. [5]State Key Laboratory of Biogeology and Environmental Geology, China University of Geosciences, Wuhan, P.R. China. [6]Geophysical Institute, University of Bergen, Bergen, Norway. [7]Nansen Environmental and Remote Sensing Centre, Bjerknes Centre for Climate Research, Bergen, Norway. [8]NORCE Norwegian Research Centre, Bjerknes Centre for Climate Research, Bergen, Norway. [9]Centre for Early Sapiens Behaviour, University of Bergen, Bergen, Norway. [10]Plateau Atmosphere and Environment Key Laboratory of Sichuan Province, School of Atmospheric Sciences, University of Information Technology, Chengdu, China. ✉e-mail: zhongshi.zhang@pku.edu.cn

Considering this context, we conducted eight sea-level sensitivity experiments with different levels of GMSL rise, encompassing both recent historical conditions (SL0.15-0.3 m) and projected future scenarios (SL0.625 m or more, Methods). Here, GMSL rise is represented by a globally uniform uplift of the ocean reference surface—an idealized but scientifically justified simplification[4]. In all SL experiments, GMSL rise was imposed at the start of the simulation and remained fixed throughout the integration. We also performed one pre-industrial (PI) control run and one experiment without sea-level rise (SL0m). All experiments were run for 2200 model years, with analyses focusing on the last 200 years of the model output.
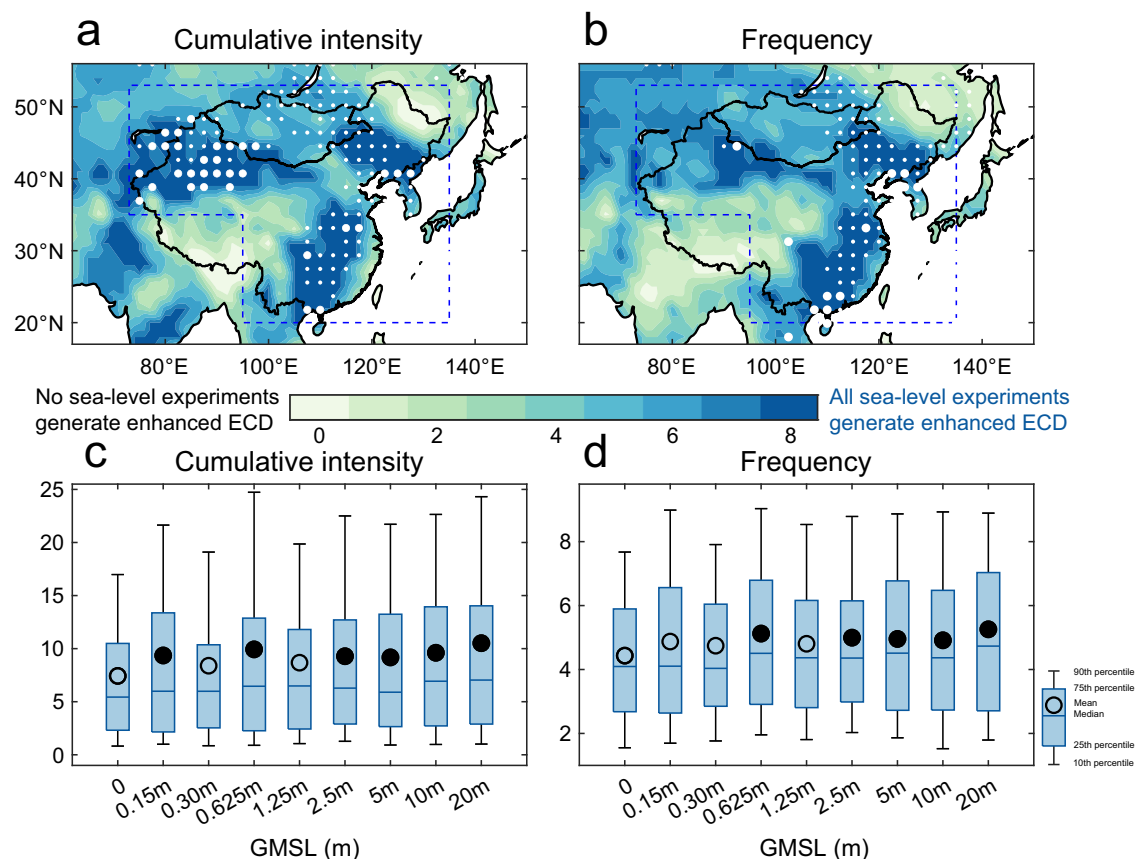
Results

Increased winter extreme cold events in East Asia

Our sensitivity experiments have revealed that as GMSL rises, East Asia experiences a greater intensity and higher frequency of extreme cold days (ECDs) (Fig. 1a, b). ECDs are defined as days with mean temperatures below the 10th percentile (Methods). When GMSL rise is below 0.3 m, the intensification of ECDs remains limited (Fig. 1a, b large dots). A GMSL rise of 0.625 m marks the onset of significant increases in both cumulative intensity and frequency (Fig. 1a, b small dots). When GMSL rise exceeds 1.25 m, the increases in both metrics remain consistently significant (Fig. 1c, d). However, it is important to note that the relationship between the response of ECDs and sea-level rise is non-linear (Supplementary Fig. 1-3).

Synoptic-scale atmospheric responses to GMSL

Extreme cold events in mid-high latitudes are often associated with the generation and maintenance of blocking anticyclones characterized by a weakening of mid-latitude westerly winds on sub-seasonal timescales (10–20 days). Here, our experiments reveal that the sea level rise can cause prolonged persistence of blocking circulation and associated cold extremes in East Asia. Analyses utilizing Self-Organizing Maps[26] (SOM, Methods) show that a specific synoptic pattern (SOM1, Fig. 2a) in winter favors the ECDs occurrence in East Asia (Fig. 2b). The SOM1 field exhibits a north-positive/south-negative dipole at 500 hPa geopotential height, similar to a blocking circulation (compare Fig. 2a and Supplementary Fig. 4). Compared to the SL0m, the frequency and max persistence of SOM1 increases in almost all sea-level experiments (Fig. 2c). The increase in max persistence can be significant (90% confidence level) even when the GMSL uplift is only tens of centimeters (Fig. 2c asterisk). Although the behavior in SOM1 is non-linear, the consistent increase in frequency and max persistence provides robust evidence showing the influence of GMSL rise on the synoptic scale. Meanwhile, the other two patterns (SOM2 and SOM3), which reduce East Asian winter ECDs, have their frequency and max persistence declining in most sea-level experiments (Supplementary Fig. 5).

Further SOM analyses demonstrate the SOM1 field consists of three clusters related to blocking, with a positive geopotential height anomaly appearing over Northern Europe in SOM1.1 (Supplementary Fig. 6d), over the Ural Mountains in SOM1.2 (Supplementary Fig. 6e),

Fig. 1 | Intensification in extreme cold events due to global mean sea level rise.
a The number of sea-level experiments that generate increased cumulative intensity of winter (DJF) extreme cold days at each land model grid. All results are based on the 200-year mean of each experiment. **b** As in (**a**), but for frequency. The large dots indicate that in the SL0.15 m/0.3 m, significant changes are simulated in each land model with a confidence level greater than 90% (t-test). The small dots indicate additional regions where significant changes emerge in the SL0.625 m. The stippling indicates that at least one (small do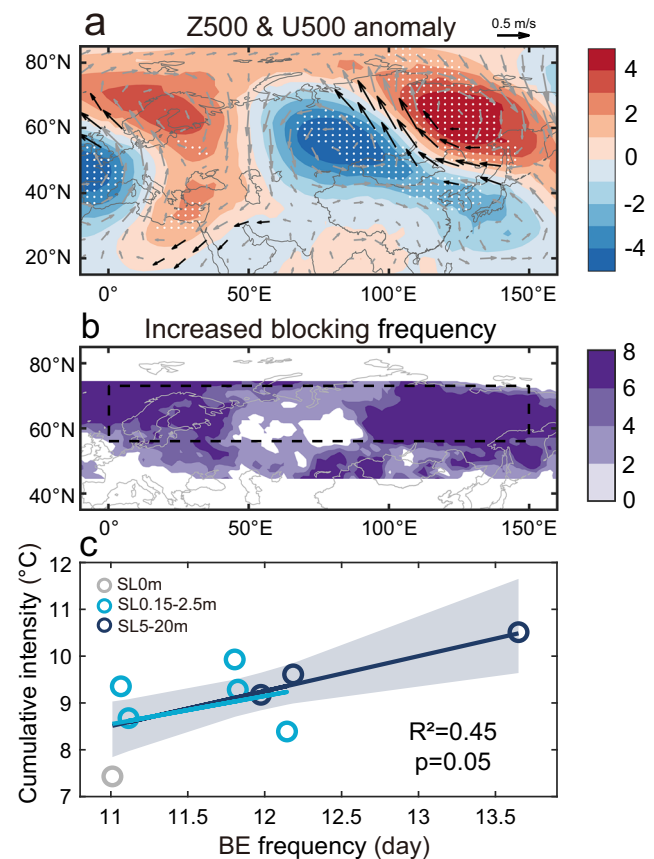ts) and two (large dots) sets of low sea level rise experiments (SL0.15-0.625 m) simulate a significant change with a confidence level greater than 90% (t-test) at each land model. **c**, **d** display the cumulative intensity and frequency, regionally averaged in the deep blue regions within the box surrounded by black dash lines in (**a**) and (**b**). The solid (hollow) dots indicate the mean change is significant (insignificant) at a 90% confidence level (t-test) compared to the SL0m experiment. Note the cumulative intensity and frequency from our pre-industrial experiment are 17.6 °C and 9 days; the cumulative strength results are taken as absolute values for better demonstration.
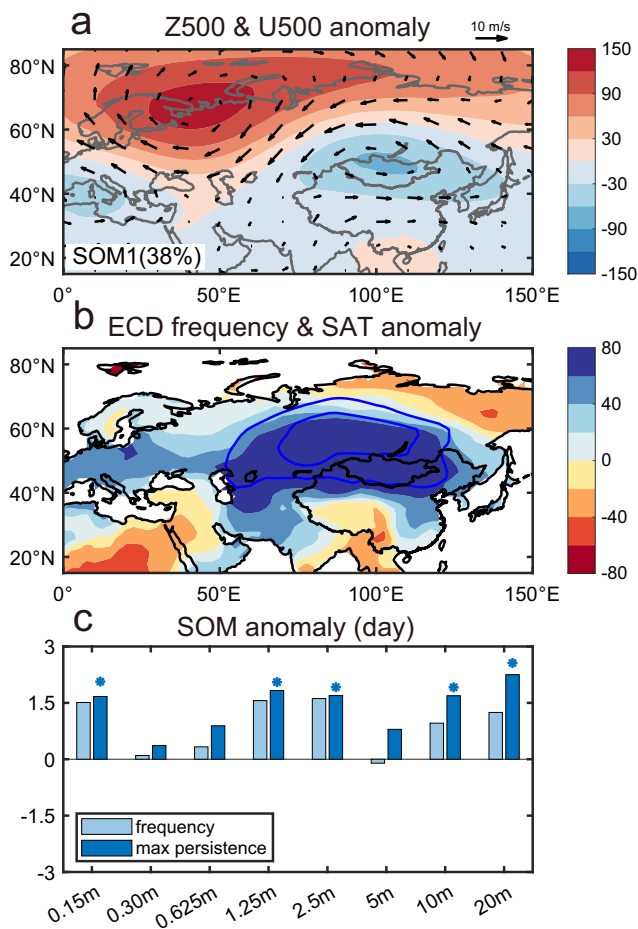
Fig. 2 | Specific atmospheric circulation field favoring extreme cold days in East Asia. The Eurasian winter circulation patterns in the sea-level experiments are divided into three clusters (SOM1, SOM2, SOM3) at a synoptic scale. **a** The winter (DJF) anomalies in geopotential height (shade, gpm) and wind (arrows) fields at 500 hPa in SOM1. **b** The changes in frequency of extreme cold days (shading, %) and surface air temperature (contours of −2 and −4 °C) under SOM1. **c** The variations in the frequency and max persistence (days) of SOM1 in the sea-level rise experiments relative to SL0m. The asterisk indicates a significant change (90% confidence level with t-test) in the mean value compared to SL0m. All results are based on the 200-year mean of each experiment.


Fig. 3 | Relationships between blockings and extreme cold events. a The anomalies in geopotential height (shading, gpm) and wind (arrows) fields at 500 hPa, composited in the sea-level experiments in winter, relative to SL0m. The stippling on shading and black arrow indicate that all sea-level experiments agree with the sign of the ensemble mean anomalies. The results of each experiment are shown in Supplementary Fig. 9. **b** The number of sea-level experiments that generate an increased blocking frequency at each land model grid in winter (DJF). The increase in blocking frequency in Northern Europe and Eastern Siberia consistently corresponded with the increase in SOM1.1 and SOM1.3 across all sea-level experiments. **c** The linear regression between the frequency of blocking events in 0–150°E, 55–75°N, and cumulative intensity of extreme cold days in East Asia. The light/deep blue lines show the linear fits by the SL0-2.5/0–20 m experiments, and the shadows show a 90% confidence interval. All results are based on the 200-year mean of each experiment.

and over Eastern Russia in SOM1.3 (Supplementary Fig. 6f). They correspond to three important typical blockings: high-latitude European blocking[27], Ural blocking[28], and Okhotsk blocking[28]. These blockings reinforce the trough-ridge structure over Eurasia for an extended period—a week or even longer—thus allowing more transport of cold air masses from the Arctic into East Asia[28–34]. Compared to the SL0m, the frequency of SOM1.1 and SOM1.3 enhances in most sea-level experiments, whereas the appearance of SOM1.2 is more dominant in the SL0.3 m and SL2.5 m experiments (Supplementary Fig. 6g).

The increased occurrence of blocking events (BE) over Eurasian mid-high latitudes explains much of the intensification in East Asian ECDs. As sea-level rise, winter background westerly winds weaken (Fig. 3a), allowing larger-scale eddies to become stationary[35], which favors the development of BE (Fig. 3b and Supplementary Fig. 7). Meanwhile, the mid-latitude potential vorticity gradient weakens with rising sea-level, suggesting a more non-linear response of BE[36]. The heightened occurrence of BE in these regions can explain up to ~45% of enhanced ECDs cumulative intensity ($R^2 = 0.45$, Fig. 3c), as well as ~49% of the heightened ECDs frequency ($R^2 = 0.49$, Supplementary Fig. 8). Notably, even when excluding the effect of high sea-level rise

experiments (0–2.5 m), our conclusion is still robust (light blue lines in Fig. 3c).

Hemispheric-scale atmospheric responses

The weakening of westerly winds in Eurasian mid-latitudes is closely connected to the significant warming in the North Pacific (Supplementary Fig. 10), driven by rising sea-level. This surface warming can generate significant positive geopotential height anomalies through both thermal and eddy forcing (Supplementary Fig. 11), thereby triggering an eastward-propagating Rossby waves—a mechanism supported by prior studies[37,38]. As a result, wave-train-like anomalies appear at the Northern Hemisphere mid-high latitudes (Fig. 4a). A positive geopotential height anomaly extends from Northern Europe to Eastern Russia, while a negative anomaly develops over East Asia, indicating a weakening of both the westerly winds and the meridional potential vorticity gradient in the mid-high latitudes. These anomalies exhibit an equivalent barotropic structure (compare Fig. 3a and Fig. 4a), consistent with previous results due to the North Pacific surface warming[39].
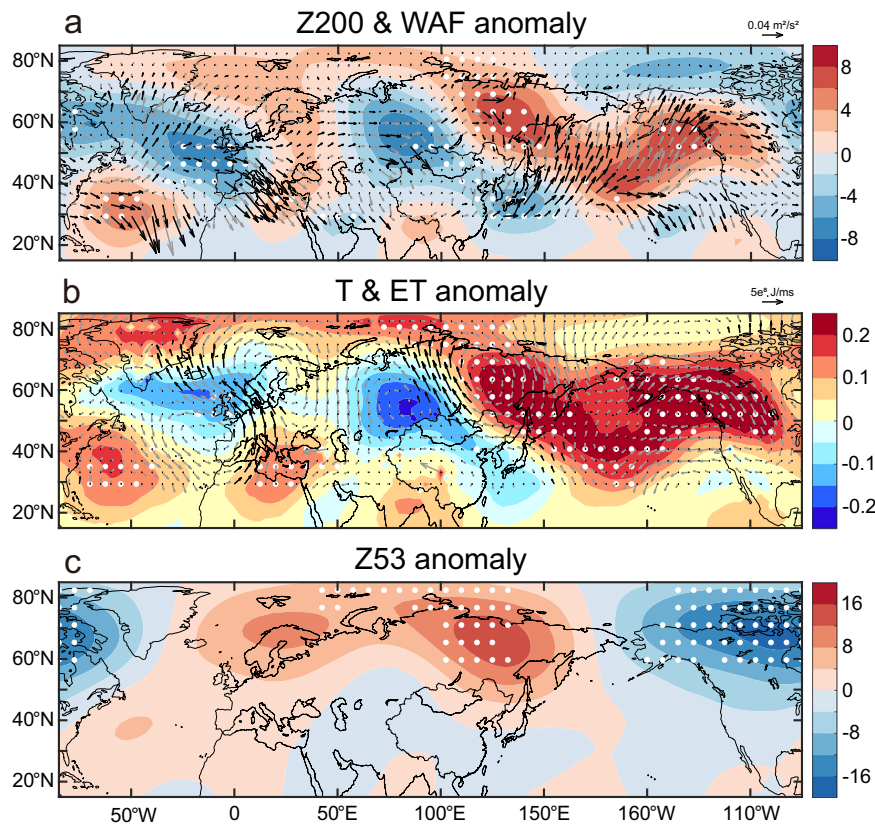
Fig. 4 | Adjustments in large-scale atmospheric circulation. a The anomalies in the 200 hPa geopotential height (shading, gpm) and horizontal wave activity flux (arrows, using the climatological wind of SL0m as the background wind), composited in the sea-level experiments in winters, relative to SL0m. **b** As in (**a**), but for the average temperature (shading, °C) and atmosphere energy transport (ET, arrows) between 850 hPa and 500 hPa. **c**, As in (**a**), but for the geopotential height at 53 hPa. The stippling on shading and black arrow indicate that all sea-level experiments agree with the sign of the ensemble mean anomalies. The results of each experiment are shown in Supplementary Figs. 12–14. All results are based on the 200-year mean of each experiment.

Meanwhile, such responses in large-scale atmospheric circulations strengthen the poleward atmospheric energy transport, contributing to the regional warming of the Arctic. When sea-level rises, the anticyclonic anomaly over Eastern Siberia transports more energy into the Arctic near 100°E (Fig. 4b black arrows). This enhanced poleward energy transport can warm the Arctic troposphere while cooling the East Asian troposphere[40] (Fig. 4b shading), which reduces poleward temperature gradient, thus favoring the weakened westerly wind as well as the enhanced occurrence of BE.

In addition, another response due to the North Pacific warming appears in the polar vortex (Fig. 4c). Due to the weakened zonal wavenumber-1 waves in response to North Pacific warming (Supplementary Fig. 15), the polar vortex shifts towards North America and away from the Eurasian continent[41–43], further promoting blocking events and enhancing cold air intrusion in East Asia[36,42,44].

Atmosphere-only experiments

Our atmosphere-only experiments affirm the significant influence of North Pacific warming on ECDs in East Asia (Methods, Supplementary Table 1). When winter sea surface temperature (SST) anomalies from the North Pacific are introduced without additional modifications in these atmosphere-only experiments, a notable intensification of ECDs emerges (Fig. 5). Remarkably, these responses remain significant even when utilizing winter SST anomalies from coupled experiments featuring small GMSL rise in centimeters (Fig. 5 white dot).

Furthermore, our atmosphere-only experiments confirm the key mechanisms driving the intensification of ECDs. The experiments reveal a decrease in westerly winds and an increase in BE in the mid-high latitudes of Eurasia (Fig. 6), resulting in intensification of ECDs.

These changes are closely linked to tropospheric wave-train-like anomalies, Arctic warming, and polar vortex shift, driven by North Pacific warming (Supplementary Fig. 18).

Discussion

Our study highlights the effect of GMSL rise on synoptic systems. Even a small uniform sea-level uplift – one aspect of GMSL rise – can promote stronger and more frequent winter extreme cold events in East Asia. Furthermore, this study suggests that the responses of winter extreme cold events are probably nonlinear within the magnitude of current and projected GMSL change by the end of this century. The non-linear relationship is related to the variable circulation pattern, partly stemming from the inherent complexity of the climate system, such as the nonlinear changes in SST[4,45] and blocking events[46].

Considering the GMSL rise, the potential significance of North Pacific warming in influencing winter extreme cold events in East Asia in the future becomes evident. In our coupled sea-level experiments, the simulated North Pacific warming correlates with enhanced northward oceanic heat transport and a linear increase in water flow through the Bering Strait[4] (Supplementary Fig. 20). These simulated changes appear robust and are further supported by recent data indicating a rising net water flux through the Bering Strait in -0.010 Sv/year[47].

At the same time, several limitations of our simulations should be acknowledged. First, our coupled sea-level experiments have been conducted over a span of 2200 years, a duration sufficient to induce substantial warming in the North Pacific. In the upcoming century, the warming in this region due to sea-level rise may exhibit a slower rate and a smaller magnitude. Second, while our simulations effectively capture the long-term responses to GMSL rise, they do not account for
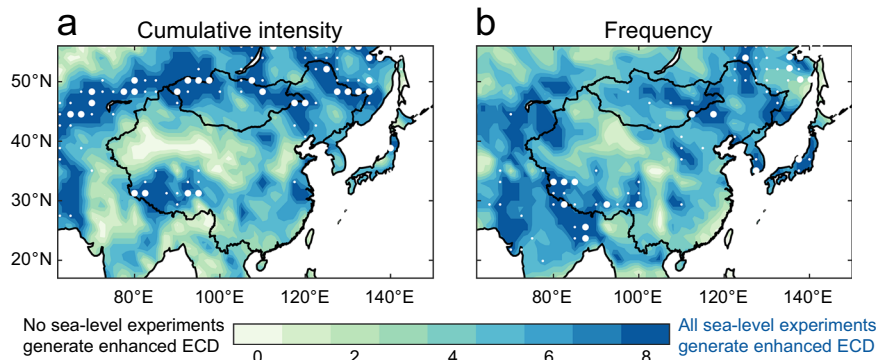
Fig. 5 | Intensification in extreme cold events due to North Pacific warming.
a, b Similar to Fig. 1a, b. Here, we conducted nine atmosphere-only experiments (corresponding to sea-level rise 0–20 m, Methods). By applying the winter monthly average sea surface temperature anomaly to CAM4, we obtained the consistent intensification of extreme cold over East Asia. The results of each experiment are shown in Supplementary Figs. 16–17. These experiments run for 45 years, with analysis focusing on the final 40 years.
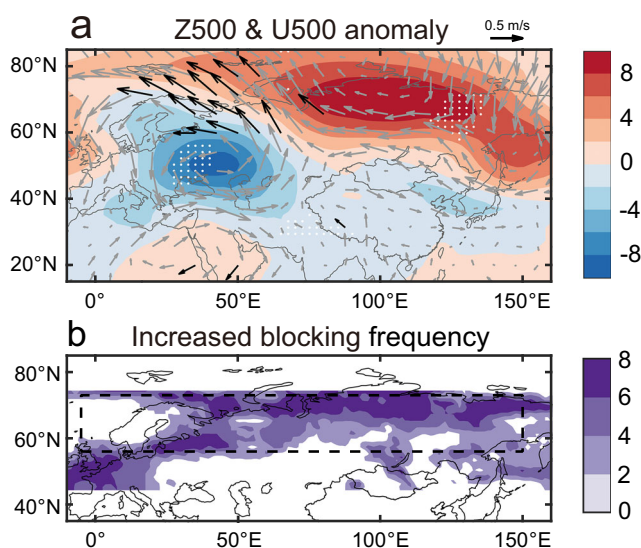
Fig. 6 | Atmospheric circulation anomaly due to North Pacific warming.
a, b Similar to Fig. 3a, b, but for the result of atmosphere-only experiments. We observe that North Pacific warming leads to a uniform increase in the blocking frequency across Eurasian mid-high latitudes. This suggests that the reduced blocking frequency in the Ural region under sea-level rise (Fig. 3b)−less favorable for extreme cold events in East Asia−may be influenced by other factors, such as the cooling in North Atlantic and Barents-Kara Seas[9]. The results of each experiment are shown in Supplementary Fig. 19. All results are based on the 40-year mean of each experiment.

transient responses. Third, we used a uniform sea-level rise and did not account for regional differences (Supplementary Fig. 21). Results from our additional atmosphere-only experiment suggest that regional sea-level variations may also influence winter extreme cold events in East Asia, although the effects appear minor and less significant (Supplementary Fig. 22). Fourth, in scenarios with much higher GMSL rise (e.g., greater than 2.5 m, which is unlikely to occur within the next century), atmospheric CO_2 concentrations are expected to far exceed 400 ppm. The warming caused by high CO_2 levels and the associated increase in climate system variability could potentially offset the effects of sea-level rise. Nevertheless, ongoing concerns regarding the influence of sea-level rise cannot be dismissed. As time progresses, the enduring impacts of GMSL rise are likely to become increasingly prominent.

Our study underscores that the threats arising from rising sea levels are not limited to coastal regions alone but extend to inland areas.

In addition to extreme cold events, adjustments to ocean circulation prompted by sea-level rise may affect natural variability (such as Pacific Decadal Oscillation) associated with other extreme weather events. Meanwhile, sea-level rise contributing to warming at high latitudes, particularly over Greenland, could expedite the onset of climate tipping points. Thus, the risks associated with sea-level rise are global in scope. Moreover, the processes through which sea-level rise influences the global climate are more complicated than simply lifting the sea-level datum. Further studies on sea-level rise require the development of a new generation of climate models. Given that sea-level rise will continue to rise throughout this century, an urgent assessment of the global disaster risk stemming from sea-level rise is imperative.

Methods
Introduction to NorESM1-F
NorESM1-F is a computationally efficient version of the Norwegian Earth System Model family[48]. It was built upon the Community Climate System Model, version 4, and developed based on the version for the fifth phase of the Coupled Model Intercomparison Project (CMIP5), NorESM1-M. Like NorESM1-M, NorESM1-F uses the same atmosphere-land grid with a horizontal resolution of 2° but has a new tripolar grid with a nominal 1° horizontal resolution for the ocean-sea-ice components. The tripolar grid provides a higher horizontal resolution (~40 km) and is more isotropic at high northern latitudes. There are 26 vertical levels in the atmosphere and 53 vertical layers in the ocean component, respectively.

Experimental design
We designed ten simulations, PiControl, CO2400, CO2400sl0.15m, CO2400sl0.3m, CO2400sl0.625m, CO2400sl1.25m, CO2400sl2.5m, CO2400sl5m, CO2400sl10m and CO2400sl20m (Supplementary Table 1, use abbreviations in the main text). Sea-level rise is implemented by lowering topography and increasing bathymetry (Supplementary Table 1). In all sea-level experiments, CO_2 concentration and sea-level rises are imposed at the start of the simulation and remain fixed throughout the integration. In all SL experiments, atmospheric CO_2 concentration was fixed at 400 ppm (close to current levels) to isolate the impact of GMSL rise. All sea-level experiments run for 2200 model years, and we analyze the model output for the last 200 years. Here, we only introduce the three newly added experiments: CO2400, CO2400sl0.15m, and CO2400sl0.3m. For more other experiments, please see Zhang et al.[4].

In CO2400, the atmospheric CO_2 level is 400 ppm, and all other boundary conditions (including orbital parameters, CH_4 level, bathymetry, and topography) are identical to the PiControl experiment.

CO_2400 is initialized from the Levitus[49] temperature and salinity and run for 2200 model years, which is different from the original 1700-year-long CO_2400 experiment[3] initialized from the PiControl experiment. Due to different initialization and integration lengths, CO_2400 and CO_2400original exhibit differences in the simulated SST. But no matter which CO_2400 experiment is used, the key mechanism that intensifies extreme cold events over East Asia−North Pacific warming−remains robust (Supplementary Fig. 23).

In $CO_2400sl0.15$ m and $CO_2400sl0.3m$, we consider a GMSL rise of 0.15,0.30 m (close to present) in sea level experiments. Except for the ocean bathymetry and topography height, all other boundary conditions are identical to the previous sea level experiments[4].

Atmosphere-only experiments

We designed nine atmosphere-only simulations to verify the effect of warming North Pacific. The control run is forced by climatological SST annual cycle of the CO_2400 experimental. In the sensitive run, monthly North Pacific SST anomalies obtained from the 200-year mean (Supplementary Fig. 10 red box) of SL0.15-20 m are added onto the climatological SST from December to February. In addition, we conducted an atmosphere-only experiment to assess the influence of regional sea-level (rsl) anomalies. These anomalies were derived from satellite altimetry-based sea surface height data over 1993–2023, with the global mean removed to isolate spatial patterns, and imposed as changes in surface geopotential height (PHIS). All experiments are integrated for 45 model years. We analyze the model outputs in the last 40 model year. For the threshold of extreme cold events, we use the same values as the coupled experiments analysis.

Extreme cold event

We define the temperature threshold by the 10th percentile of the winter daily surface air temperature (SAT) distribution of the PiControl experiment (following Kolstad et al.)[50]. An extreme cold day is identified for each grid point when the SAT is below the threshold.

For the intensity of extreme cold events, we use the cumulative intensity, which refers to the integration of SAT anomaly at each grid point:

$$\text{cumulative intensity} = \sum_{3}^{\text{day}} \left(SAT_{anomaly} \right) \quad (1)$$

The cumulative intensity is helpful as it integrates intensity and persistence in a single number. Note that we count extreme cold events lasting 3/5 days or longer, the results are taken as absolute values for better demonstration. In the main text, we show the results of the 3 days, and the results of the 5 days are shown in the Supplementary Fig. 3.

Atmospheric blocking

Following Scherrer et al.[51] and Davini et al.[52], we adopt gradient-reversal (REV) indices to identify blocking events. A 2D extension of the blocking index is defined by:

$$GHGS\ (\lambda, \phi) = \frac{Z(\lambda, \phi) - Z(\lambda, \phi_S)}{\phi - \phi_S} \quad (2)$$

$$GHGN\ (\lambda, \phi) = \frac{Z(\lambda, \phi_N) - Z(\lambda, \phi)}{\phi_N - \phi} \quad (3)$$

$$GHGS2\ (\lambda, \phi) = \frac{Z(\lambda, \phi_S) - Z(\lambda, \phi_S - 15°)}{15°} \quad (4)$$

$$\phi_N = \phi + 15°, \phi_S = \phi - 15° \quad (5)$$

where $\lambda\ (\phi)$ is the longitude (latitude) at a given grid point. $\lambda\ (\phi)$ ranges in longitudes from 0°-360° (latitudes 45°-70°N); and $Z(\lambda, \phi)$ is the daily 500 hPa geopotential height at the grid point (λ, ϕ). It is considered as an instantaneous blocking when the grid point (λ, ϕ) satisfies the following formula:

$$GHGS\ (\lambda, \phi) > 0\ \text{m/1}° \quad (6)$$

$$GHGN\ (\lambda, \phi) < -10\ \text{m/1}° \quad (7)$$

$$GHGS2\ (\lambda, \phi) < -5\ \text{m/1}° \quad (8)$$

The blocking frequency at a given grid is defined as the percentage of the days of instantaneous blocking divided by the total number of days for the winter.

For the blocking events, we define the area of the instantaneous blocking in the region (0–150°E, 55–75°N) that exceeds at least $5.0 \times 10^5\ \text{km}^2$ within a $10° \times 10°$ sliding window and lasts at least 5 days (similar to Woollings et al.)[34].

SOM

Self-Organizing Maps[26] (SOM) projects a non-linear mapping of a high-dimensional input vector onto a regularly arranged topological low-dimensional array. This method, extensively used in atmospheric sciences in recent decades, is effective in characterizing large-scale circulation patterns and identifying their possible impacts on weather and climate extremes[53,54]. The SOM program used here is the Python miniSOM library.

We carry out SOM clustering in two rounds. For the first round, we select winter (DJF) daily 500 hPa geopotential height from CO_2400 and eight sea-level experiments over the domain 0–150°E, 35–85°N in the data pool to carry out SOM analyses, obtaining three clusters (cold East Asia SOM1, warm East Asia SOM2, and general East Asia SOM3). Then, we only select the 500 hPa geopotential height chosen into the SOM1 cluster in the data pool to conduct SOM clustering for the second round (Supplementary Fig. 5). We have tested several SOM arrays, including 1×2, 1×3, and 2×2. The 1×3 node is sufficient to represent the range of large-scale circulation patterns and is easily distinguishable.

Due to the inherent stochasticity of the SOM, multiple random runs are recommended. Here, we use 10 random runs to select the SOM array that better represents the input data. The similarity of the SOM clusters to the contained data vectors is expressed using the quantization error[55]:

$$\text{quantization error} = \frac{1}{N} \sum ||x_i - m_{x_i}|| \quad (9)$$

where N is the number of data-vectors and m_{x_i} is the best matching prototype of the corresponding x_i data-vector.

Atmospheric energy transport

The total energy transport in a unit air column from 1000 hPa to 500 hPa follows the equation given by Graversen et al[40].

$$ET = \frac{1}{g} \int_{1000}^{500} \mathbf{v} * \left(C_p T + Lq + gz + k \right) dp \quad (10)$$

The atmospheric energy includes the internal energy ($C_p T$), the latent energy (Lq), the potential energy (gz), and the kinetic energy (k). Here,

v is wind velocity vector, C_p is specific heat capacity for constant volume, T is absolute temperature, L is the specific heat of condensation of sublimation, q is specific humidity, g is gravity, and z is height; while p_s and p_O represent surface pressure and upper-level pressure.

Potential vorticity gradient

Potential vorticity gradient (PV$_y$) is a key influence on blocking activity[46]. Under the lower-PV$_y$ background condition, the blocking event has weaker energy dispersion and stronger nonlinearity so that it exhibits longer persistence, slower decay and weaker eastward movement. The PVy in the barotropic atmosphere is expressed as:

$$PV_y = \beta - \bar{u}_{yy} + F\bar{u} \tag{11}$$

where β is the meridional gradient of planetary vorticity, $\bar{u}$ is the basic zonal wind, and F is the barotropic Froude number.

Data availability

The winter mean data including frequency and cumulative intensity of extreme cold events, blocking frequency, air temperature, wind, geopotential height, and sea surface temperature from the sea-level experiments are publicly available on Zenodo (https://zenodo.org/records/16909285). More model output can be provided, upon request, from the author C.D. (caoyi@cug.edu.cn).

Code availability

The NorESM code is available on GitHub (https://github.com/NorESMhub/NorESM).

References

1. Fox-Kemper, B. et al. Ocean, cryosphere, and sea level change. in Climate Change 2021: The Physical Science Basis. Contribution of Working Group I to the Sixth Assessment Report of the Intergovernmental Panel on Climate Change (eds. Masson-Delmotte, V. et al.) vol. 9 1211–1362 (Cambridge University Press, 2021).
2. Hu, A. & Bates, S. C. Internal climate variability and projected future regional steric and dynamic sea level rise. *Nat. Commun.* **9**, 1068 (2018).
3. Sweet, W. V. & Park, J. From the extreme to the mean: acceleration and tipping points of coastal inundation from sea level rise. *Earth's Future* **2**, 579–600 (2014).
4. Zhang, Z. et al. Atmospheric and oceanic circulation altered by global mean sea-level rise. *Nat. Geosci.* **16**, 321–327 (2023).
5. Kug, J.-S. et al. Two distinct influences of Arctic warming on cold winters over North America and East Asia. *Nat. Geosci.* **8**, 759–762 (2015).
6. Zhang, R., Zhang, R. & Dai, G. Intraseasonal contributions of Arctic sea-ice loss and Pacific decadal oscillation to a century cold event during early 2020/21 winter. *Clim. Dyn.* **58**, 741–758 (2022).
7. He, S., Xu, X., Furevik, T. & Gao, Y. Eurasian Cooling Linked to the Vertical Distribution of Arctic Warming. *Geophys. Res. Lett.* **47** https://doi.org/10.1029/2020gl087212 (2020).
8. Zheng, F. et al. The 2020/21 extremely cold winter in China influenced by the synergistic effect of La Niña and Warm Arctic. *Adv. Atmos. Sci.* **39**, 546–552 (2022).
9. Zhang, X. et al. Extreme cold events from East Asia to North America in Winter 2020/21: comparisons, causes, and future implications. *Adv. Atmos. Sci.* **39**, 553–565 (2022).
10. Yao, Y., Zhang, W., Luo, D., Zhong, L. & Pei, L. Seasonal cumulative effect of Ural blocking episodes on the frequent cold events in China during the early winter of 2020/21. *Adv. Atmos. Sci.* **39**, 609–624 (2022).
11. Zhang, R., Screen, J. A. & Zhang, R. Arctic and Pacific Ocean conditions were favorable for cold extremes over Eurasia and North America during winter 2020/21. *Bull. Am. Meteorol. Soc.* **103**, E2285–E2301 (2022).
12. Yao, Y. et al. Extreme cold events in North America and Eurasia in November-December 2022: a potential vorticity gradient perspective. *Adv. Atmos. Sci.* **40**, 953–962 (2023).
13. Yang, H. & Fan, K. The causes of intraseasonal alternating warm and cold variations over China in Winter 2021/22. *J. Clim.* **37**, 5153–5170 (2024).
14. Cohen, J. et al. Recent Arctic amplification and extreme midlatitude weather. *Nat. Geosci.* **7**, 627–637 (2014).
15. Cohen, J. et al. Divergent consensuses on Arctic amplification influence on midlatitude severe winter weather. *Nat. Clim. Change* **10**, 20 (2020).
16. Chuan, F. & Bing-Yi, W. Enhancement of winter Arctic warming by the Siberian high over the past decade. *Atmos. Ocean. Sci. Lett.* **8**, 257–263 (2015).
17. Outten, S. et al. Reconciling conflicting evidence for the cause of the observed early 21st century Eurasian cooling. *Weather and Climate Dynamics Discussions*, 1–32 (2022).
18. Screen, J. A., Deser, C., Simmonds, I. & Tomas, R. Atmospheric impacts of Arctic sea-ice loss, 1979-2009: separating forced change from atmospheric internal variability. *Clim. Dyn.* **43**, 333–344 (2014).
19. Sun, L., Perlwitz, J. & Hoerling, M. What caused the recent "Warm Arctic, Cold Continents" trend pattern in winter temperatures?. *Geophys. Res. Lett.* **43**, 5345–5352 (2016).
20. Blackport, R., Screen, J. A., van der Wiel, K. & Bintanja, R. Minimal influence of reduced Arctic sea ice on coincident cold winters in mid-latitudes. *Nat. Clim. Change* **9**, 697–704 (2019).
21. McCusker, K. E., Fyfe, J. C. & Sigmond, M. Twenty-five winters of unexpected Eurasian cooling unlikely due to Arctic sea-ice loss. *Nat. Geosci.* **9**, 838 (2016).
22. Takaya, K. & Nakamura, H. Geographical dependence of upper-level blocking formation associated with intraseasonal amplification of the Siberian high. *J. Atmos. Sci.* **62**, 4441–4449 (2005).
23. Takaya, K. & Nakamura, H. Mechanisms of intraseasonal amplification of the cold Siberian high. *J. Atmos. Sci.* **62**, 4423–4440 (2005).
24. Gao, R. L., Zhang, R. H., Wen, M. & Li, T. R. Interdecadal changes in the asymmetric impacts of ENSO on wintertime rainfall over China and atmospheric circulations over western North Pacific. *Clim. Dyn.* **52**, 7525–7536 (2019).
25. Clark, J. P. & Lee, S. The role of the tropically excited arctic warming mechanism on the warm arctic cold continent surface air temperature trend pattern. *Geophys. Res. Lett.* **46**, 8490–8499 (2019).
26. Kohonen, T. The self-organizing map. *Proc. IEEE* **78**, 1464–1480 (1990).
27. Luo, D., Yao, Y. & Dai, A. Decadal relationship between European blocking and the North Atlantic Oscillation during 1978–2011. Part I: Atlantic Conditions. *J. Atmos. Sci.* **72**, 1152–1173 (2015).
28. Hwang, J., Son, S.-W., Martineau, P. & Barriopedro, D. Impact of winter blocking on surface air temperature in East Asia: Ural versus Okhotsk blocking. *Clim. Dyn.*, 1–16 (2022).
29. Blackport, R. & Screen, J. A. Insignificant effect of Arctic amplification on the amplitude of midlatitude atmospheric waves. *Sci. Adv.* **6**, eaay2880 (2020).
30. Barnes, E. A., Dunn-Sigouin, E., Masato, G. & Woollings, T. Exploring recent trends in Northern Hemisphere blocking. *Geophys. Res. Lett.* **41** (2014).
31. You, C., Tjernstrom, M., Devasthale, A. & Steinfeld, D. The role of atmospheric blocking in regulating arctic warming. *Geophys. Res. Lett.* **49**, e2022GL097899 (2022).
32. Luo, D. et al. Impact of Ural blocking on winter warm Arctic–cold Eurasian anomalies. Part I: Blocking-induced amplification. *J. Clim.* **29**, 3925–3947 (2016).

33. Luo, B., Wu, L., Luo, D., Dai, A. & Simmonds, I. The winter midlatitude-Arctic interaction: effects of North Atlantic SST and high-latitude blocking on Arctic sea ice and Eurasian cooling. *Clim. Dyn.* **52**, 2981–3004 (2019).

34. Woollings, T. et al. Blocking and its response to climate change. *Curr. Clim. Change Rep.* **4**, 287–300 (2018).

35. Hoskins, B. & Woollings, T. Persistent extratropical regimes and climate extremes. *Curr. Clim. Change Rep.* **1**, 115–124 (2015).

36. Huang, J., Hitchcock, P., Maycock, A. C., McKenna, C. M. & Tian, W. Northern hemisphere cold air outbreaks are more likely to be severe during weak polar vortex conditions. *Commun. Earth Environ.* **2**, 147 (2021).

37. Hu, D. & Guan, Z. Decadal relationship between the stratospheric Arctic vortex and Pacific decadal oscillation. *J. Clim.* **31**, 3371–3386 (2018).

38. Fang, J. & Yang, X.-Q. Structure and dynamics of decadal anomalies in the wintertime midlatitude North Pacific ocean–atmosphere system. *Clim. Dyn.* **47**, 1989–2007 (2016).

39. Park, J.-H., An, S.-I. & Kug, J.-S. Interannual variability of western North Pacific SST anomalies and its impact on North Pacific and North America. *Clim. Dyn.* **49**, 3787–3798 (2017).

40. Graversen, R. G., Mauritsen, T., Tjernström, M., Källén, E. & Svensson, G. Vertical structure of recent Arctic warming. *Nature* **451**, 53–56 (2008).

41. Hu, D., Guan, Z., Tian, W. & Ren, R. Recent strengthening of the stratospheric Arctic vortex response to warming in the central North Pacific. *Nat. Commun.* **9**, 1697 (2018).

42. Zhang, J., Tian, W., Chipperfield, M. P., Xie, F. & Huang, J. Persistent shift of the Arctic polar vortex towards the Eurasian continent in recent decades. *Nat. Clim. Change* **6**, 1094–1099 (2016).

43. Svendsen, L., Keenlyside, N., Bethke, I., Gao, Y. & Omrani, N.-E. Pacific contribution to the early twentieth-century warming in the Arctic. *Nat. Clim. Change* **8**, 793–797 (2018).

44. Hamouda, M. E., Portal, A. & Pasquero, C. Polar vortex disruptions by high latitude ocean warming. *Geophys. Res. Lett.* **51**, e2023GL107567 (2024).

45. Luo, B., Luo, D., Dai, A., Simmonds, I. & Wu, L. Decadal variability of winter warm Arctic-cold Eurasia dipole patterns modulated by Pacific decadal oscillation and Atlantic multidecadal oscillation. *Earth's. Future* **10**, e2021EF002351 (2022).

46. Luo, D., Zhang, W., Zhong, L. & Dai, A. A nonlinear theory of atmospheric blocking: a potential vorticity gradient view. *J. Atmos. Sci.* **76**, 2399–2427 (2019).

47. Woodgate, A. & Peralta-Ferriz, R. C. Warming and freshening of the pacific inflow to the Arctic from 1990-2019 implying dramatic shoaling in Pacific Winter Water ventilation of the Arctic water column[J]. *Geophys. Res. Lett.* **48**, e2021GL092528 (2021).

48. Guo, C. et al. Description and evaluation of NorESM1-F: A fast version of the Norwegian Earth System Model (NorESM). *Geosci. Model Dev.* **12**, 343–362 (2019).

49. Levitus, S. & Boyer, T. P. World ocean atlas 1994 volume 4: temperature. In NOAA Atlas NESDIS (US Government Printing Office, 1994).

50. Kolstad, E. W., Breiteig, T. & Scaife, A. A. The association between stratospheric weak polar vortex events and cold air outbreaks in the Northern Hemisphere. *Q. J. R. Meteorol. Soc.* **136**, 886–893 (2010).

51. Scherrer, S. C., Croci-Maspoli, M., Schwierz, C. & Appenzeller, C. Two-dimensional indices of atmospheric blocking and their statistical relationship with winter climate patterns in the Euro-Atlantic region. *Int. J. Climatol.* **26**, 233–249 (2006).

52. Davini, P., Cagnazzo, C., Gualdi, S. & Navarra, A. Bidimensional diagnostics, variability, and trends of northern hemisphere blocking. *J. Clim.* **25**, 6496–6509 (2012).

53. Horton, D. E. et al. Contribution of changes in atmospheric circulation patterns to extreme temperature trends. *Nature* **522**, 465–469 (2015).

54. Rousi, E., Kornhuber, K., Beobide-Arsuaga, G., Luo, F. & Coumou, D. Accelerated western European heatwave trends linked to more-persistent double jets over Eurasia. *Nat. Commun.* **13**, 1–11 (2022).

55. Rousi, E., Anagnostopoulou, C., Tolika, K. & Maheras, P. Representing teleconnection patterns over Europe: a comparison of SOM and PCA methods. *Atmos. Res.* **152**, 123–137 (2013).

Acknowledgements

Author contributions

Z.Z. designed and performed the simulations. C.D. performed the data analysis and wrote the draft of the paper. N.K., S.P.S., and O.H.O. contributed to the analyses of atmospheric dynamics. A.B., J.X., R.P.R., Y.L., B.L., and M.W. contributed to interpreting the results. All authors contributed to reviewing and editing the paper.

Competing interests

The authors declare no competing interests.

Additional information

Supplementary information The online version contains supplementary material available at https://doi.org/10.1038/s41467-025-63727-1.

Correspondence and requests for materials should be addressed to Zhongshi Zhang.

Peer review information *Nature Communications* thanks Dehai Luo and the other anonymous reviewers for their contribution to the peer review of this work. A peer review file is available.

Reprints and permissions information is available at http://www.nature.com/reprints

Publisher's note Springer Nature remains neutral with regard to jurisdictional claims in published maps and institutional affiliations.